Examination of VLC-PUFA–Deficient Photoreceptor Terminals

Lea D. Bennett,[1,2] Blake R. Hopiavuori,[2,3] Richard S. Brush,[2,4] Michael Chan,[2,4] Matthew J. Van Hook,[5] Wallace B. Thoreson,[5,6] and Robert E. Anderson[1–4]

[1]Department of Cell Biology, University of Oklahoma Health Sciences Center, Oklahoma City, Oklahoma, United States
[2]Dean McGee Eye Institute, Oklahoma City, Oklahoma, United States
[3]Oklahoma Center for Neuroscience, University of Oklahoma Health Sciences Center, Oklahoma City, Oklahoma, United States
[4]Department of Ophthalmology, University of Oklahoma Health Sciences Center, Oklahoma City, Oklahoma, United States
[5]Department of Ophthalmology and Visual Sciences, University of Nebraska Medical Center, Omaha, Nebraska, United States
[6]Department of Pharmacology and Experimental Neuroscience, University of Nebraska Medical Center, Omaha, Nebraska, United States

Correspondence: Robert E. Anderson, Department of Ophthalmology, University of Oklahoma Health Sciences Center, 608 S. L. Young Boulevard, Oklahoma City, OK 73104, USA; Robert-Anderson@ouhsc.edu.

Submitted: January 21, 2014
Accepted: April 11, 2014

Citation: Bennett LD, Hopiavuori BR, Brush RS, et al. Examination of VLC-PUFA–deficient photoreceptor terminals. *Invest Ophthalmol Vis Sci*. 2014;55:4063–4072. DOI:10.1167/iovs.14-13997

Purpose. Juvenile-onset autosomal dominant Stargardt-like macular dystrophy (STGD3) is caused by mutations in *ELOVL4* (elongation of very long fatty acids-4), an elongase necessary for the biosynthesis of very long chain fatty acids (VLC-FAs $\geq$ C26). Photoreceptors are enriched with VLC polyunsaturated fatty acids (VLC-PUFAs), which are necessary for long-term survival of rod photoreceptors. The purpose of these studies was to determine the effect of deletion of VLC-PUFAs on rod synaptic function in retinas of mice conditionally depleted (KO) of *Elovl4*.

Methods. Retina function was assessed in wild-type (WT) and KO by electroretinography. Outer plexiform structure was evaluated by immunofluorescence and transmission electron microscopy. Single-cell recordings measured rod ion channel operation and rod bipolar glutamate signaling. Sucrose gradient centrifugation was used to isolate synaptosomes from bovine retina. Proteins and lipids were analyzed by Western blotting and tandem mass spectroscopy, respectively.

Results. Inner retinal responses (b-wave, oscillatory potentials, and scotopic threshold responses) of the ERG were decreased in the KO mice compared to controls. However the rod ion channel operation and bipolar glutamate responses were comparable between groups. Biochemical analysis revealed that conventional and ribbon synapses have VLC-PUFAs. Ultrastructural analysis showed that the outer plexiform layer was disorganized and the diameter of vesicles in rod terminals was smaller in the KO mice.

Conclusions. Very long chain PUFAs affect rod function by contributing to synaptic vesicle size, which may alter the dynamics of synaptic transmission, ultimately resulting in a loss of neuronal connectivity and death of rod photoreceptors.

Keywords: VLC-PUFA, ELOVL4, STDG3

A juvenile form of macular degeneration, autosomal dominant Stargardt-like macular dystrophy (STGD3), is characterized by a loss of central vision at an early age. Mutations in the gene associated with STGD3, elongation of very long chain fatty acids-4 (*ELOVL4*),[1–5] cause a frame shift in the *ELOVL4* transcript that introduces a premature stop codon and results in a truncated ELOVL4 protein that has lost its endoplasmic reticulum (ER) retention/retrieval signal. The truncated protein does not get targeted to the ER, the site of very long chain polyunsaturated fatty acids (VLC-PUFAs; 26–40 carbons[6–8]) synthesis. The mutant protein has no enzymatic activity,[9] so it could be that the loss of VLC-PUFAs is involved in the STGD3 disease pathogenesis. Although the *ELOVL4* gene is expressed in the skin, brain, testis, and retinal photoreceptor cells,[10] the skin contains very long chain saturated fatty acids (VLC-FAs),[11,12] whereas the sperm cells and the retina are enriched in VLC-PUFAs.[13,14]

Although we know that retinal VLC-PUFAs are incorporated in phosphatidylcholine in photoreceptor outer segment membranes,[15] their role in the retina remains unclear. In our companion paper[16] we showed that absence of VLC-PUFAs in the neural retina revealed an unexpected and potentially novel role in synaptic transmission in rod photoreceptors. Absence of these fatty acids led to a reduction in the b-wave of the rod-mediated photoresponse and a slow death of rod cells over time. To elucidate the role of VLC-PUFAs in photoreceptor terminals, we conditionally deleted *Elovl4* in rod and cone photoreceptors of mice and measured inner retina function, synaptic connectivity, and ultrastructure of rod terminals with reduced VLC-PUFAs.

Materials and Methods

Materials

Primary antibodies used were Bassoon (Enzo Life Sciences, Farmingdale, NY, USA), VGlut1 (UC Davis/National Institutes of

Health; Clone N28/9), synaptic vesicle protein (SV2[17]; gift from Erik Floor, University of Kansas), PKCα (Cell Signaling, Danvers, MA, USA), and rhodopsin (RET-P1; Abcam, Cambridge, MA, USA). Horseradish-conjugated secondary antibodies (rabbit polyclonal and mouse monoclonal) were from Pierce Scientific (Rockford, IL, USA). Fluorescein-conjugated anti-rabbit antibodies –488 and anti-mouse –594 or –647 were from Invitrogen (Grand Island, NY, USA). Peanut agglutinin-594 (PNA) and Vectashield mounting medium with 4′,6-diamidino-2-phenylindole (DAPI; H-1200) were purchased from Vector Laboratories (Burlingame, CA, USA). All solvents for lipid analysis were HPLC grade. Lipid internal standards used for tandem mass spectrometry (MS) analysis were 14:0/14:0 phosphatidylcholine (PC), 14:0/14:0 phosphatidylethanolamine (PE), and 14:0/14:0 phosphatidylserine (PS; Avanti Polar Lipids, Alabaster, AL, USA).

Animals

See companion manuscript[16] for details on the breeding scheme used to generate the *Chx10-Cre*$^{+}$*/Elovl4*$^{flox/flox}$ mice. Mice were killed as described in the companion paper.[16] All procedures were performed in accordance with the ARVO Statement for the Use of Animals in Ophthalmic and Vision Research and the University of Oklahoma Health Sciences Center Guidelines for Animals in Research. All protocols were reviewed and approved by the Institutional Animal Care and Use Committees of the University of Oklahoma Health Sciences Center and the Dean McGee Eye Institute.

Immunofluorescence

Immunofluorescence labeling was performed on paraffin-embedded 5-week, 9-month, and 12-month-old mouse retinal sections using standard procedures described earlier[18] to visualize the PKCα, Bassoon, and VGlut1 expression. Each antibody was applied at 1:100; secondary antibodies were used at 1:1000, and DAPI was used at 1:5000. Slides were viewed on a FV-500 Olympus confocal microscope, and the images were acquired with Flow View software (Olympus America, Center Valley, PA, USA). Contrast and brightness were adjusted with Photoshop (Adobe Systems, Inc., San Jose, CA, USA).

Synaptosome Isolation

Synaptosomes were isolated from fresh bovine retinas by a modified protocol adapted from published methods.[19,20] Briefly, bovine whole retinas (WR) were dissected, homogenized (three retinas per tube; $n = 4$), and centrifuged two times in a discontinuous sucrose gradient to remove outer segment (OS) membranes. The remaining material was centrifuged (150*g*) to pellet and discard nuclei and cellular debris. The supernatant was centrifuged at 800*g* to pellet and remove the ribbon synaptosomes (RS) and then again (25,000*g*) to pellet and collect the conventional synaptosomes (CS). The WR, OS, RS, and CS fractions were immunoblotted to verify purification as described below. Lipid analysis of OS, RS, and CS fractions was performed using tandem MS as described below. The percent total VLC-PUFA–containing PC molecular species detected in each purified fraction was normalized to the net intensity of rhodopsin (per microgram protein) to account for contamination from OS membranes in the synaptic fractions. Ratios were averaged ($n = 4$) for each fraction (OS, RS, and CS).

Western Blot Analysis

Homogenized bovine WR and purified OS, RS, and CS fractions were loaded (1.25, 5, or 10 μg protein) from preparations described above. SDS-PAGE and Western blotting were performed using standard methods. Blots were visualized with a Kodak Imager. Carestream imaging software (Carestream Health, Inc., Rochester, NY, USA) was used to measure rhodopsin levels in synaptosome fractions.

Tandem Mass Spectrometry Analysis of Retina Lipids (MS/MS)

Retinal lipids were extracted as previously described.[21] Further details are provided in the companion manuscript.[16]

Electroretinography

Mice were prepared as described previously[22] and in the companion paper.[16] Oscillatory potentials (OPs) were extracted by digitized filtration from ERG responses of dark-adapted 12-month-old mice. Low (100 Hz)- and high (300 Hz)-pass filters were applied to ERG responses. Time between test flashes was increased to ensure rod recovery between flashes. The four OP wavelets filtered from responses to increasing light intensities (0.001–1000 cd·s/m^2) were summed and represent a function of light intensity. The response time for the OPs was determined as the latency of the dominant wavelet (OP2) after flash stimulation to 0.1 cd·s/m^2. Butterworth filters (30 and 80 Hz) were incorporated to remove the amplitude contamination from the a- and b-waves. The filtered responses were Fourier transformed into a power spectrum density for the light intensity 0.1 cd·s/m^2 to determine the frequency of the OPs.[23]

Scotopic threshold responses (STR) from dark-adapted 12-month-old mice were acquired from 50 flashes of light (–3.3 to –6.3 log scot cd·s/m^2) over 600 ms. Amplitude of response (nV/ms) was averaged for each genotype and plotted for comparison.

Whole-Cell Recording in Retinal Slices

Protocols for whole-cell recording in mouse retinal slices were approved by the Institutional Animal Care and Use Committee at the University of Nebraska Medical Center. To make retinal slices for whole-cell recordings, 12-month-old wild-type (WT) or KO mice were killed by CO_2 asphyxiation. After enucleation, the eye was hemisected and the retina mounted (vitreal side down) on a nitrocellulose membrane (5 × 10 mm; type AAWP, 0.8-μm pores; Millipore, Billerica, MA, USA). The retina was cut into 125-μm slices using a razor blade tissue slicer (Stoelting, Wood Dale, IL, USA). Slices were rotated 90° to view the retinal layers and were anchored in the recording chamber by embedding the ends of the nitrocellulose membrane in vacuum grease. The recording chamber was mounted on an upright fixed-stage microscope (Nikon E600FN [Nikon, Melville, NY, USA] or Olympus BH2 [Center Valley, PA, USA]), and the slices were constantly superfused at ~1 mL/min with room temperature Ames' medium (United States Biological, Salem, MA, USA) bubbled with 95% O_2 and 5% CO_2.

Whole-cell voltage clamp recordings were performed with either an Axon 200B or Multiclamp 700A amplifier (Molecular Devices, Sunnyvale, CA, USA), and currents were acquired using a Digidata 1322A or 1440A interface and pClamp software (Molecular Devices). To record from rods, we targeted somata in the proximal half of the outer nuclear layer (ONL). Rods were voltage clamped at –70 mV, and calcium currents (I_{Ca}) were recorded with a voltage ramp protocol (–90 to +60 mV, 0.5 mV/ms). Currents were leak subtracted using P/8 protocols. Voltage dependence of I_{Ca} was measured by fitting with a Boltzmann function. Because rod I_{Ca} were typically small, we performed analysis on averages of 2 to 10

traces from individual cells. The pipette solution for rod recordings contained (mM) 145 gluconic acid, 145 CsOH, 3 $MgCl_2$, 1 $CaCl_2$, 3.5 NaCl, 1 adenosine triphosphate (ATP)-Mg, 0.5 guanosine triphosphate (GTP)-Na, 10 HEPES, and 3 EGTA. The pH was adjusted to 7.3 with CsOH, and the osmolality was 272 mOsm.

To record from rod bipolar cells (RBCs), we targeted large somata in the distal inner nuclear layer (INL). Recorded cells were confirmed as RBCs[24] by filling with sulforhodamine B dye (0.5 mg/mL; Sigma-Aldrich, St. Louis, MO, USA) during whole-cell recording, and non-RBCs were excluded from analysis. In addition to sulforhodamine B, the pipette solution for RBC recordings contained (mM) 125 gluconic acid, 125 CsOH, 3 $MgCl_2$, 1 $CaCl_2$, 3.5 NaCl, 1 ATP-Mg, 0.5 GTP-Na, 10 HEPES, and 20 1,2-bis(o-aminophenoxy) ethane-N,N,N′,N′-tetraacetic acid. The pH was adjusted to 7.3 with CsOH, and the osmolality was 275 mOsm. Rod bipolar cells were voltage clamped at –60 mV, and the retinal slices were bathed in the mGluR6 agonist L-(+)-2-amino-4-phosphonobutyric acid (L-AP4, 4 μM; Tocris, Minneapolis, MN, USA). Rod bipolar cell transduction currents were evoked with a 1-second puff of (*RS*)-α-cyclopropyl-4-phosphonophenyl glycine (CPPG, 600 μM; Tocris)[25] delivered to the outer plexiform layer (OPL) from a patch pipette using a custom-made pressure ejector (3–4 psi). Analysis of response amplitude was performed on averages of two to six CPPG current traces from individual cells.

Electron Microscopy

Transmission electron microscopy (TEM) was performed on 12-month-old mice as described in our companion manuscript.[16] Images were taken at ×5000 and ×10,000 and randomly coded for quantification. Care was taken to harvest the eyes at the same time of day, ~1 to 2 hours after the onset of light.

Statistical Analyses

Statistical analyses were performed by using GraphPad Prism 5.0 software (GraphPad Software, Inc., La Jolla, CA, USA). Student's two-tailed *t*-test was performed for OP fast Fourier transform and TEM comparisons. One-way ANOVA was performed for analysis of lipid species by MS/MS. Bonferroni's multiple comparison post hoc test was performed with a 95% confidence interval to determine statistical significance at $P < 0.05$.

Results

Rod-Mediated Function Deteriorated in 12-Month-Old VLC-PUFA–Deficient Mice

Synaptic communication between the different retinal neurons was analyzed by various components of the ERG. Representative scotopic ERG response traces showed that 9-month-old KO mice had smaller a- and b-wave amplitudes over a spectrum of increasing light intensities (–3.0 log cd·s/m^2 to 3.0 log cd·s/m^2) compared to 12-month-old WT responses to the same light stimulations (Figs. 1A, 1B). Additionally, it appears as if the VLC-PUFA–deficient response did not return to baseline as quickly as the WT responses, especially at the higher light intensities. By filtering these responses we were able to measure the OPs of these mice (Figs. 1C, 1D). These wavelets are thought to originate from feedback responses of the amacrine, horizontal, and bipolar cells mediated by the rod photoresponse.[26] The 9-month-old KO OP wavelet amplitudes (Fig. 1D) were decreased compared to the 12-month-old WT responses (Fig. 1C). To show the relation of the OP amplitudes and the b-wave, their summed amplitudes were plotted against increasing light intensities (Fig. 1E). The power density spectrum of the OP response was lower in the KO compared to WT, but the frequency (Fig. 1F) and latency (KO = 35.7 ± 1.2 ms and WT = 34.2 ± 1.0 ms; $n = 10$) did not differ between the two groups. Taking the presence of VLC-PUFAs in synaptosomes together with the report, these data provide evidence that VLC-PUFAs are important for rod-mediated pathways involving inner retinal neurons.

The STR is a postreceptor response generated by the proximal retina, namely, the ganglion cells, and is mediated by the Müller cell membrane potentials.[27–29] We found that the STR response amplitudes from the 12-month-old WT mice were higher than those of the 9-month-old KO mice to increasing light intensities (–3.3 to –6.3 log cd·s/m^2; Figs. 1G, 1H, respectively). This indicated that the inner retina cells were not receiving the upstream signals from the photoreceptors with reduced VLC-PUFAs.

Rod I_{Ca} and RBC Glutamate Receptor Currents Do Not Depend on VLC-PUFA

Because changes in photoreceptor synaptic transmission can arise from alterations of presynaptic voltage-gated calcium currents (I_{Ca}), we used whole-cell patch clamp recordings to study both the amplitude and voltage dependence of rod I_{Ca} in retinal slices from WT and *Elovl4* KO mice (Figs. 2A–C). Rods were voltage clamped at –70 mV, and I_{Ca} was evoked with a ramp from –90 to +60 mV (0.5 mV/ms). The I_{Ca} amplitude was similar in WT and KO mice (WT = 6.6 ± 1.1 pA, $n = 11$; KO = 6.4 ± 2.1 pA, $n = 12$; $P = 0.93$). The voltage dependence of I_{Ca} was also similar in WT and KO mice; in WT mice, I_{Ca} peaked at –10.2 ± 2.0 mV. In KO mice, the peak was –12.5 ± 3.9 mV ($P = 0.60$). Additionally, the half-maximal voltage of activation (V_{50}) was –31.1 ± 1.1 mV in WT mice and –30.0 ± 1.5 mV in KO mice ($P = 0.58$). These results indicate that I_{Ca}, which regulates synaptic transmission in rods and cones, was not altered by the reduction in retinal VLC-PUFAs in the *Elovl4* KO mice.

To test whether the changes in synaptic transmission might instead result from postsynaptic effects of retinal VLC-PUFA reduction, we examined RBC transduction by puffing the mGluR6 antagonist, CPPG (600 μM), onto RBC dendrites in the presence of bath-applied L-AP4 (4 μM; Figs. 2D–F). When RBCs were voltage clamped at –60 mV, this triggered an inward current of similar amplitude in both WT (8.6 ± 1.2 pA, $n = 10$) and KO mice (10.0 ± 3.0 pA, $n = 12$). These values were not significantly different ($P = 0.68$). Together, these results suggest that the changes in synaptic transmission from rods to downstream retinal neurons involve presynaptic deficits in the release mechanism independent of I_{Ca}.

Mice With Reduced VLC-PUFAs Had Synaptic Reorganization

To examine the synaptic connectivity between photoreceptor and bipolar cells, we performed immunofluorescence on 5-week-old and 9-month-old WT and KO mouse retinas. There were no differences at 5 weeks of age in the immunostaining of the ribbon protein Bassoon (green) and bipolar cell-labeled with PKCα (orange; Fig. 3A). It is important to note that the green labeling in the lower OPL is indicative of a blood vessel and is the result of cross-reaction of the secondary antibody. Glutamatergic vesicles labeled by VGlut1 (green) were found in the ONL, photoreceptor terminals in the OPL, and INL of WT and KO mice at 5 weeks of age (Fig. 3B). The VGlut1 labeling

Investigative Ophthalmology & Visual Science

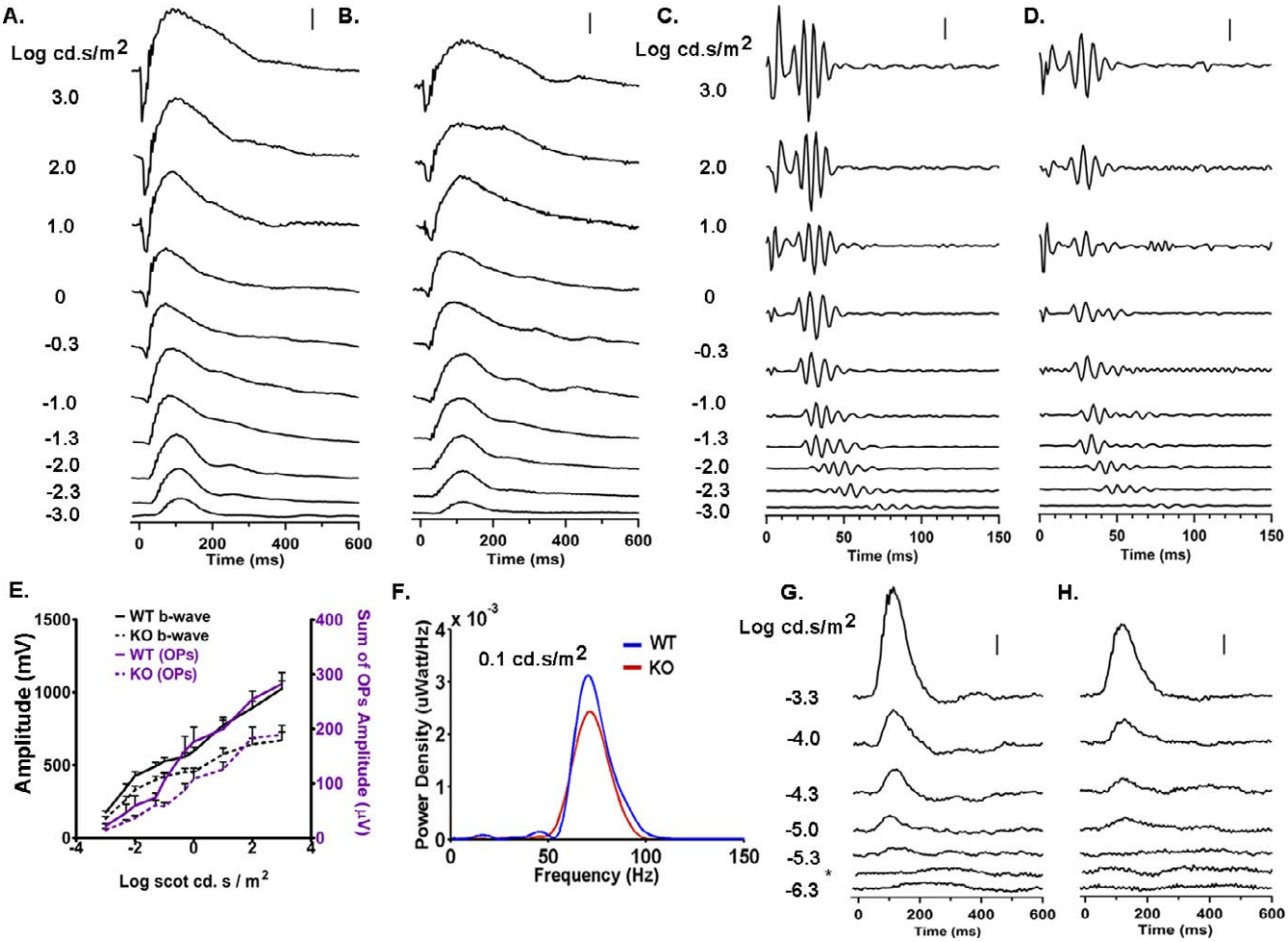

Figure 1. Rod-mediated function deteriorated in VLC-PUFA–deficient mice. Representative 12-month-old WT (**A**) responses to increasing light intensities (–3.0 log scot cd·s/m^2 to 3.0 log scot cd·s/m^2) had higher a- and b-wave amplitudes than 9-month-old KO (**B**) responses. *Vertical bar* at *upper right* in each case is *y*-axis amplitude = 200 μV. (**C**) WT oscillatory potentials (OPs) had amplitudes higher than the KO (**D**) OP amplitudes. *Vertical bar* at *upper right* in each case is *y*-axis amplitude = 20 μV. The numbers between the traces in (**A**, **C**) are the light intensities (log scot cd·s/m^2) at which the responses were elicited. The latency of the OP responses was not different between the mice. (**E**) The sum of the four OP amplitudes in (**C**, **D**) and simultaneously recorded b-wave responses (**A**, **B**) to increasing light intensities were lower in the KO mice compared to the WT mice (n = 12 WT and 11 KO). Data are represented as the mean ± SEM. (**F**) The power density spectrum but not the frequency was lower in the KO mice compared to WT (representative spectrum from n = 8 WT and 5 KO). (**G**) Representative scotopic threshold responses (STR) to increasing light intensities (–6.3 log scot cd·s/m^2 to –3.3 log scot cd·s/m^2) from 12-month-old WT and (**H**) 9-month-old KO showed that the STR amplitudes were lower in the KO mice compared to WT. *6.0 log scot cd·s/m^2. *Vertical bar* at *upper right* in each case is *y*-axis amplitude = 20 μV.

appeared to be localized preferably to the ONL in the KO mice, but the WT retina showed VGlut1 preferential staining in the OPL (Fig. 3B).

At 9 months the Bassoon (green) was ectopically located (arrowheads) in the ONL of the KO retina, unlike the WT retina, where Bassoon was found in the OPL (Figs. 4A, 4B). The bipolar dendrites labeled with PKCα (red) were found in the OPL of the 5-week-old WT and KO mice, but appeared to extend into the ONL in the 9- and 12-month-old KO retina compared to the littermate control (Figs. 4A–C).

Glutamatergic vesicles labeled by VGlut1 (green) were found in the photoreceptor terminals in the OPL of WT mice, whereas VGlut1 was found in the ONL, OPL, and INL of the KO retina (Fig. 4D). The OPL in the KO retinas appeared disrupted and unorganized compared to the WT. Again, bipolar cell dendrites (arrows; orange) were found extending into the ONL of the VLC-PUFA–deficient mice compared to the WT, perhaps attempting to connect with their presynaptic targets (Fig. 4D).

Retinal Synapses Contain VLC-PUFAs

Although there were decreases in the rod b-waves, OPs, and STRs and disruption of the OPL in the VLC-PUFA–deficient mice, there were no differences in rod calcium currents or bipolar glutamate receptor currents, indicating that VLC-PUFAs might be involved in synaptic vesicle dynamics and release mechanisms in the rod terminals. To understand the role of VLC-PUFAs in retinal synapses, we first determined if these fatty acids were indeed present in photoreceptor synaptic terminals. To prepare ribbon and conventional synapses free of reactive oxygen species (ROS) contamination, we used well-established and widely published protocols.[19,20,30,31] Using fresh bovine WR, OS membranes were removed from the rest of the retina by repeated sucrose density centrifugation,[20] and RS and CS were isolated.[19] Protein analysis confirmed the isolation of the outer segments and ribbon and conventional synapses (OS, RS, and CS; Fig. 5A). Rhodopsin, an integral OS protein, was most abundant in the OS, whereas VGlut1 was

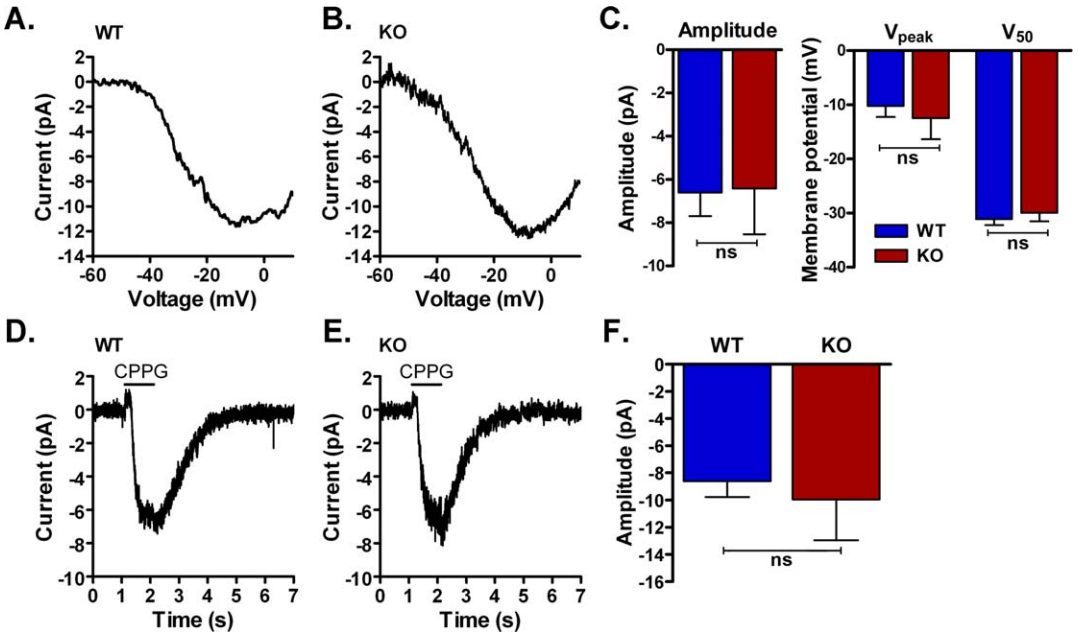

Figure 2. Rod calcium currents (I_{Ca}) and rod bipolar cell (RBC) glutamate receptor signaling were similar between 12-month-old WT and KO mice. (**A**) Representative I_{Ca} recorded with a voltage ramp (−90 to +60, 0.5 mV/ms) in a rod from a WT retina. The displayed trace is an average of two traces from a single cell. (**B**) I_{Ca} from a KO rod. The displayed trace is an average of three traces from a single cell. (**C**) *Left*: group data, showing that the I_{Ca} amplitude was similar in WT and KO rods. Likewise, the voltage dependence, as indicated by the peak voltage (V_{peak}) and voltage of half-maximal activation (V_{50}), was similar in rods from WT and KO mouse retinas. (**D**) Response of an RBC from a WT retina to a 1-second puff of CPPG (600 μM) in the presence of L-AP4 (4 μM). The RBC was voltage clamped at −60 mV, and the displayed trace is an average of five traces. (**E**) Response of an RBC from a KO retina. The displayed trace is an average of five traces. (**F**) Amplitudes of RBC responses to CPPG puffs were similar in WT and *Elovl4* KO mouse retinas. Data are mean ± SEM. ns, not significant.

localized to the ribbon synapses,[32] and synaptic vesicle protein (SV2) was found in the conventional synapse fraction[17] (Fig. 5A).

Analysis of individual PC molecular species revealed differences between the two synaptosomal fractions and ROS in several PC molecular species (Table). Phosphatidylcholine from ROS contains higher levels of saturated/monounsaturated species, whereas PC from both synaptosomal fractions contains relatively higher levels of 22:6n3-containing species. This finding corroborates Cotman et al.,[33] who first detected the presence of high levels of 22:6n3 in brain synaptosomes. To exclude VLC-PUFA contamination from the OS membranes, the VLC-PUFAs in each fraction were normalized to rhodopsin. If the VLC-PUFAs detected were simply the result of contamination by ROS membranes, the ratio (VLC-PUFAs to rhodopsin; mole %/μg) would be the same for all three preparations. The ratio of VLC-PUFA to rhodopsin was significantly higher in the synaptic fractions compared to the OS fraction (Fig. 5B), indicating that the VLC-PUFAs detected in the synaptic fractions were intrinsic to these membranes and not due to contamination from OS membranes.

Rod Ribbon Synapses of KO Mice Have Fewer Synaptic Vesicles

Taken together with the report that long chain fatty acids are enriched in synaptic vesicles,[34] we next used TEM to examine the vesicles of the photoreceptor terminals of WT and VLC-PUFA–deficient mice. Randomized TEM images were used to measure vesicle diameter in approximately 10 different terminals (50 vesicles per terminal) per individual mouse (n = 4 WT and 5 KO mice). Vesicles within the rod terminals of the WT mouse averaged 29.5 ± 0.93 nm in diameter, with the majority of vesicles between 20 and 40 nm in diameter, whereas the KO mouse vesicles averaged 24.5 ± 0.62 nm and were predominately less than 29 nm in diameter (Figs. 5C–F). The vesicles indicated by the thin arrows in Figures 5E and 5F are vesicles measured between 20 and 29 nm, and the thick arrowheads are examples of vesicles less than 20 nm in diameter. Vesicles with flat sides or vesicles that were not completely round (open arrowheads) were often seen in the KO mouse rod terminals (Fig. 5F). The number of vesicles tethered to the synaptic ribbons (25 rod ribbons/mouse) counted from single 10,000× TEM images were considered attached if they were within 40 nm of the synaptic ribbon. The WT mice had 4.7 ± 0.3 vesicles/μm ribbon whereas the KO mice had 3.6 ± 0.2 (P = 0.0405; see Figs. 5E, 5F for a representative example).

Analysis of the ultrastructure from the VLC-PUFA–deficient mouse retina revealed frequent apoptotic nuclei (white asterisks; Fig. 6A). We also observed unusually dark (arrowheads in Figs. 6A–C) and light (Fig. 6C) synaptic terminals distributed among seemingly normal rod terminals (black traced, Fig. 5A). A representative dark terminal taken at higher magnification showed typical postsynaptic process with horizontal cell (H) invaginations and the associated synaptic ribbon (Fig. 6B).

Blind analysis of approximately 100 terminals per animal showed that the WT mice had 72.3 ± 1.8% of the terminals containing postsynaptic processes (PSP) with at least one horizontal or bipolar cell dendrite, compared to 53.2 ± 4.6% (P = 0.0097) of KO rod terminals containing PSP (Fig. 6D). Figures 5E and 5F are good examples of terminals with PSP, and Figure 6B shows a terminal without PSP invagination (asterisks). Quantification of the percent of rod terminals with ribbons revealed that the WT had 61.3 ± 1.8%, whereas KO

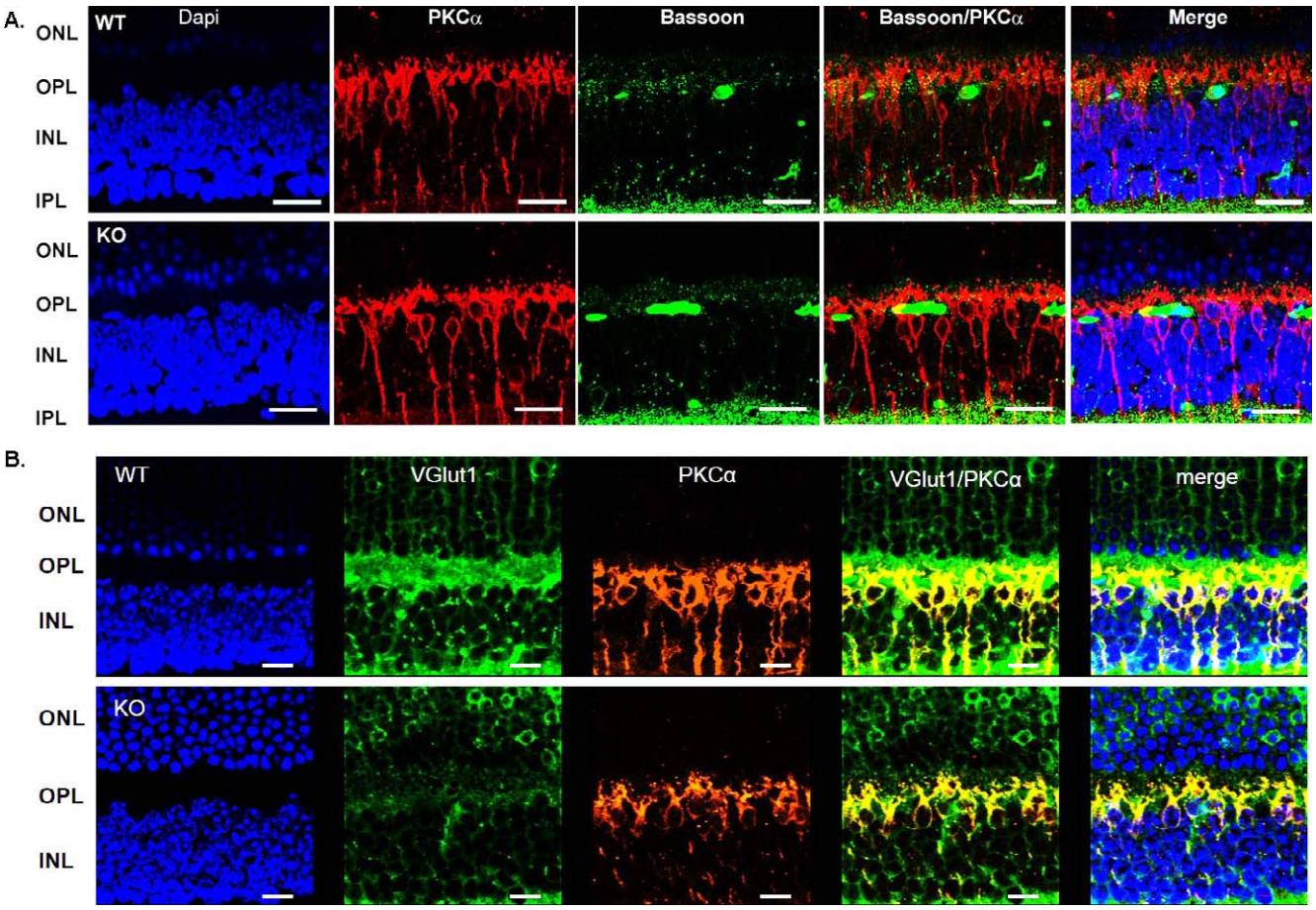

Figure 3. Reduced VLC-PUFAs caused synaptic vesicles to mislocalize in 5-week-old mouse retinas. (**A**) Ribbon protein Bassoon (*green*) was found in the outer plexiform layer along with bipolar dendrites labeled with PKCα (*red*) in the WT and KO mice. (**B**) Glutamatergic vesicles labeled with VGlut1 (*green*) preferentially localized to the OPL in the WT mice but were found predominantly in the ONL of the KO mice. *Scale bars*: 20 μm.

mice had 46.3 ± 4.3% terminals with ribbons (Fig. 6D; $P = 0.0100$). Examples of rod terminals without PSP or ribbons are indicated with black asterisks in Figure 6C.

Discussion

Here we show that VLC-PUFAs are not exclusive to photoreceptor OS, but are present in ribbon synapses as well as the smaller conventional synapses in the retina (Fig. 5B). This along with the abnormal scotopic system (Fig. 1) in the *Elovl4* KO mice indicates a novel role for VLC-PUFAs in synaptic function in the mammalian retina.

The single-cell recordings showed that receptor calcium currents and the postreceptor glutamate currents were not affected by reduced VLC-PUFAs (Fig. 3). This suggests that the reduced b-wave, OPs, and STRs in our KO mice might be attributed to a disruption in release mechanisms at synaptic ribbons. Since ELOVL4 expression is highest in the photoreceptors[2,35] and VLC-PUFAs are localized to the synaptic membranes (Figs. 5A, 5B), the most likely scenario is one in which VLC-PUFAs are incorporated into the glutamate-containing vesicles of rod terminals. Indeed, the mice with reduced VLC-PUFAs had smaller vesicles than their littermates (Figs. 5C–F). The smaller vesicles could alter the dynamics of docking and moving vesicles along the synaptic ribbon. The decrease in vesicles per ribbon in the KO mice could be explained by loss of physical interaction at the ribbon due to the smaller diameter of the VLC-PUFA–deficient vesicles. Very long chain PUFAs may increase the size of the vesicles because of their bulky polyunsaturated hydrocarbon tails, which could ultimately affect biophysical properties of the vesicles in the photoreceptor terminals. Additionally, the ultrastructure of the terminals in our mice was strikingly similar to that of synaptophysin KO mice.[36] Synaptophysin is important for synaptic vesicle formation and segregates into cholesterol-enriched microdomains of highly curved membranes.[36] Although synaptophysin KO mice had normal ERG responses, their rod terminals were interspersed with dark and light terminals and pleomorphic vesicle appearances.[36] It is important to note that the synaptophysin KO mice were reported at 9 weeks of age, whereas our VLC-PUFA–deficient mice did not show synaptic pathology at 5 weeks but showed histological defects at 9 months and similar "synaptophysin KO-like" TEM characteristics at 12 months (Figs. 3–6). It is clear from these results that VLC-PUFAs are not necessary to establish synaptic communication but are required to sustain the anatomical and physiological integrity of the rod photoreceptors. One possible correlation is that the VLC-PUFAs could be incorporated into vesicles that contain or interact with synaptic proteins that mediate endo-/exocytic activity affecting vesicle recycling pathway in the rod terminal. In the same way, reduction of VLC-PUFAs could have affected protein transport, especially if that protein were localized to the synaptic ribbon in photoreceptor terminals, as this may affect vesicle tethering or glutamate release mechanisms.

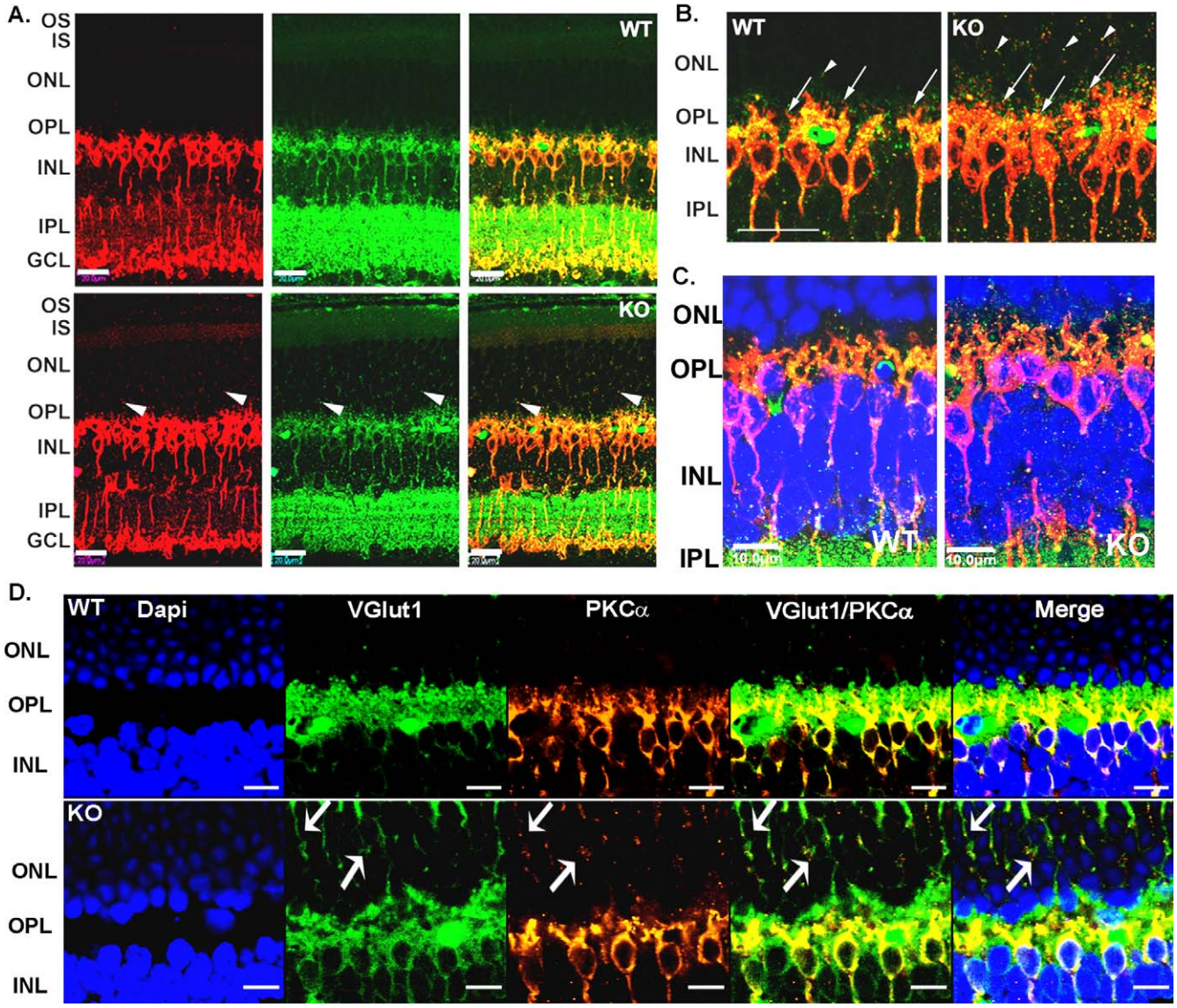

Figure 4. VLC-PUFA–deficient mice had a loss of photoreceptors and synaptic reorganization. (**A**) Representative images at low magnification showed decoration (*arrowheads*) of the outer nuclear layer (ONL) with the ribbon protein Bassoon (*green*) and bipolar dendrites labeled with PKCα (*red*) in the 9-month-old KO but not in the WT retina. (**B**) Higher magnification of the outer plexiform layer (OPL) from (**A**) showed that Bassoon (*green*) and PKCα (*red*) were localized to the OPL (*arrows*) in the WT mice, but were ectopically located in the ONL (*arrowheads*) of the KO mice. *Scale bars*: 20 μm. (**C**) High magnification of 12-month-old mouse retinas with photoreceptor ribbon and bipolar dendritic spines in the OPL of the WT mice. The KO mice showed ectopic ribbon and PCKα staining extending out of the OPL into the ONL. *Scale bars*: 20 μm. (**D**) Vesicles labeled with VGlut1 (*green*) were localized with the bipolar cell dendrites (*orange*) in the photoreceptor synaptic layer (OPL) in the WT, but were found in the ONL and OPL in the KO retina. The OPL in the KO retina was disorganized compared to WT. Similar results were observed from eight different 9-month-old mice per genotype. *Scale bars*: 10 μm. RPE, retinal pigmented epithelium; IS, inner segment; IPL, inner plexiform layer; GCL, ganglion cell layer.

Mice with absent or reduced b-wave are termed "no b-wave" (*nob*) mutants. The *nob* mice with normal a-waves and absent b-waves have mutations in postsynaptic genes that control membrane depolarization, whereas mice with mutations in presynaptic genes controlling glutamate release have normal a-waves and reduced b-waves (for a comparative review see Ref. 37). All of the presynaptic mutants are described as having abnormal or absent rod ribbons, with dendrites of inner retinal neurons extending into the ONL, and some form of ectopic photoreceptor synapses. The VLC-PUFA–deficient mice showed similar *nob* characteristics with a reduction in the number of invaginating synapses in rod terminals (Fig. 6D), as well as dendrites and synapses ectopically located in the ONL (Figs. 4, 6C, arrow). Loss of synaptic connectivity explains the sprouting of the bipolar dendrites into the ONL as they characteristically searched for a synaptic partner.[38,39] Unlike presynaptic mutant mice that have mutation in ribbon proteins, there was no difference in the ribbon localization (Bassoon) in the young animals used here (Fig. 3A). However, VGlut1 labeling in the 5-week-old mice was predominantly in the ONL of the KO mice compared to the WT mice, where VGlut1 was preferentially found in the OPL (Fig. 3B). These results suggest that development of the synaptic architecture is not dependent on the presence of VLC-PUFAs and that possible retinal remodeling precedes physiological dysfunction. We have shown here that over time the reduction of these fatty

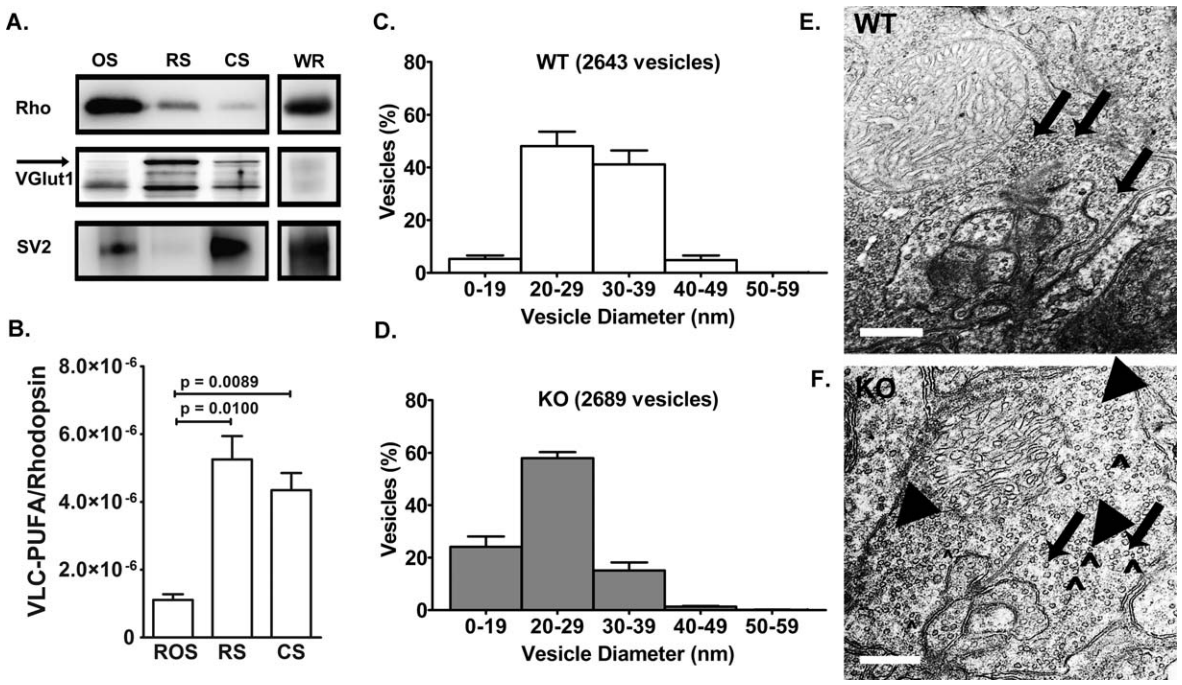

Figure 5. VLC-PUFAs are enriched in retinal synapses. (**A**) Representative Western blot of fractionated bovine whole retina (WR) showed that rhodopsin (Rho, 37 kDa) was enriched in outer segments (OS), whereas VGlut1 (60 kDa) was localized to the ribbon synaptosome (RS) and synaptic vesicle protein (SV2; 95 kDa) was localized to the conventional synaptosome (CS) fractions. The WR sample was the retinal homogenate before centrifugation. (**B**) Ribbon and conventional synaptosome (RS and CS, respectively) fractions contained VLC-PUFAs that were not derived from OS contamination ($n = 4$). (**C**) Vesicles in WT rod terminals were predominately 20 to 39 nm in diameter, whereas the vesicles within the KO mouse terminals (**D**) were more frequently 0 to 29 nm in diameter. (**E**) Representative micrograph of a WT rod terminal shows an example of vesicles measuring between 30 and 39 nm (*arrows*). (**F**) Representative micrograph of a KO rod terminal shows an example of vesicles measuring between 0 to 19 nm (*thick arrowheads*) and 30 to 39 nm (*arrows*). Abnormal vesicles (*empty arrowheads*) appearing "deflated" were frequently observed in the KO mouse spherules. Mice were 12 months of age. *Scale bars*: 500 nm. Data are expressed as mean ± SD.

acids results in retinal degeneration, synaptic reorganization, and receptor physiology dysfunction (see companion manuscript[16] and Figs. 1, 3–6). However, at this time the temporal pathology resulting from decreased VLC-PUFAs is unknown.

With regard to the reduced STR and OPs, we cannot dismiss the potential for inner retinal remodeling in the VLC-PUFA–deficient mice. Taken together with the photoreceptor-specific localization of ELOVL4,[6,40,41] our histological examination of these *Elovl4* KO mice was limited to the OPL. It is possible that some low level of expression of Elovl4 occurs in retinal cells other than rods and cones. This would not affect our claims that VLC-PUFAs are in synaptic membranes. Rather, expression of some Elovl4 activity in ganglion cells would explain why we found VLC-PUFAs in the small synaptosomes that are mostly from the inner plexiform layer and why we found decreased STR. Interestingly, when we look at lower-magnification images of Bassoon (Fig. 4A) and CtBP2 (not shown) staining, we realize that there may be some inner retinal remodeling in the VLC-PUFA–deficient mice. It will be important to follow this evidence, focusing on the inner retina structure and function in these mice.

Barabas et al.[8] recently reported that their rod-specific *Elovl4* KO mice had normal optomotor visual performance and rod b-wave responses, and concluded that VLC-PUFAs are not important for synaptic transmission. We disagree and have provided strong evidence that VLC-PUFAs are located in synaptosomes and are important for synaptic transmission from the rod photoreceptors. Furthermore, the central vision system as tested in the optomotor response can bypass synaptic pathology and provide a visual response independent of the ribbon synapse.[42] One reason the previous study did not find reduced b-wave amplitudes could be that the mice used in that study were 6 months of age, whereas the mice used in this study were 12 months of age.

The ELOVL4 protein has been well established as the elongase involved in the initial rate-limiting step in the production of VLC-PUFAs.[6–8] There has been controversy, however, surrounding the exact role of VLC-PUFAs in the retina. The results presented here support the companion manuscript[16] and clearly show that VLC-PUFAs are important for synaptic transmission by affecting shape and size of the synaptic vesicles within the rod spherules.

Table. Phosphatidylcholine Lipid Species Are Different in Retinal Synaptosomes Compared to Photoreceptor Outer Segments

	RS	CS	ROS
PC34:01, 16:0/18:1*†	12.64 ± 1.19	14.33 ± 0.94	17.29 ± 0.76
PC36:01, 18:0/18:1*†‡	4.94 ± 0.30	6.11 ± 0.37	7.38 ± 0.23
PC38:06, 16:0/22:6*†	8.88 ± 0.99	8.19 ± 0.57	5.93 ± 0.61
PC40:06, 18:0/22:6*†	15.57 ± 2.39	14.75 ± 1.86	10.35 ± 1.35
Σ VLC-PUFA†	4.51 ± 0.32	3.46 ± 0.32	5.36 ± 0.61

Σ VLC-PUFA, sum of very long chain polyunsaturated fatty acids; ROS, rod outer segments.

* RS versus ROS, $P < 0.05$.

† CS versus ROS, $P < 0.05$.

‡ RS versus CS, $P < 0.05$.

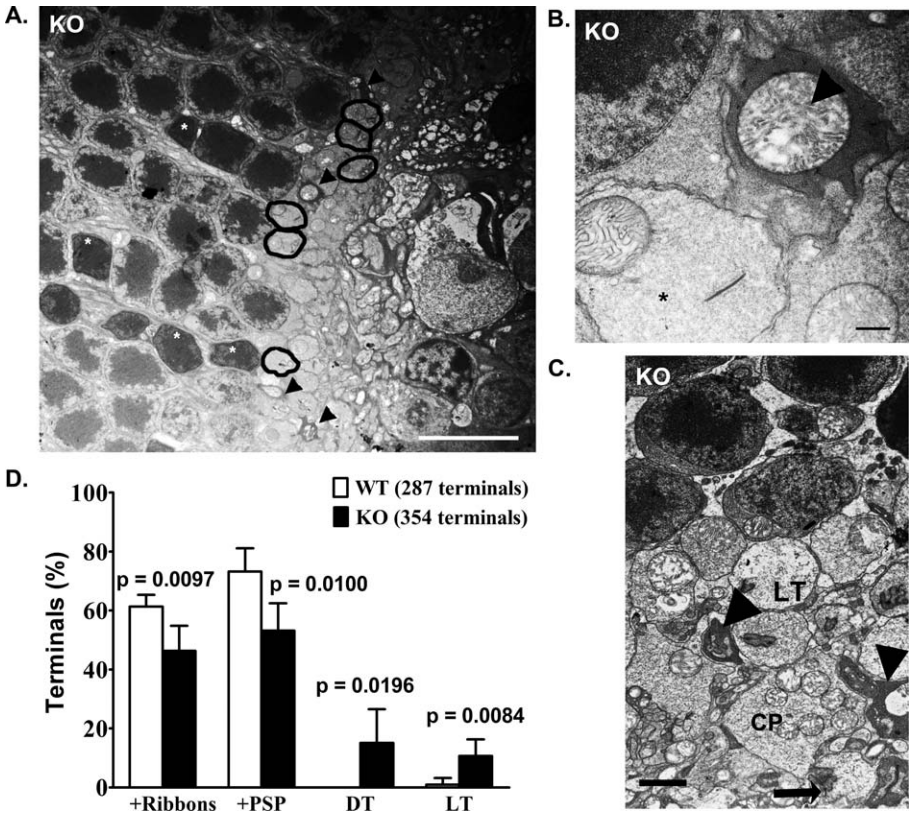

Figure 6. Mice with reduced VLC-PUFAs had abnormal rod spherules. (**A**) Ultrastructure of KO mouse retina revealed numerous apoptotic (*white asterisks*) photoreceptor nuclei and dark (*arrowheads*) terminals along with typical rod terminals (*traced*) in the OPL. *Scale bar*: 10 μm. (**B**) An example of a dark terminal found in KO OPL with invaginations from a horizontal cell and a ribbon synapse. *Scale bar*: 250 nm. (**C**) Representative micrograph from a different KO mouse with light terminals (LT), dark terminals (*thick arrowheads*), and an ectopic ribbon synapse (*arrow*) located distal to the ONL on the border of the outer OPL and the inner nuclear layer (*cropped*). Rod spherules are typically located in the proximal OPL as they are the end feet of the photoreceptor cells. The ectopic dark terminal (*bottom*) adjacent to the ectopic light terminal (*arrow*) is the terminal magnified in (**B**). CP, cone pedicle. *Scale bar*: 100 nm. (**D**) WT mice had 61.3 ± 1.8% and 73.2 ± 3.6% of their rod terminals with a synaptic ribbon or a PSP, respectively, compared to 46.3 ± 4.3% and 52.3 ± 4.6% in the KO mice. There were no dark terminals (DT) found in the WT mice, whereas 15.1 ± 5.7% DT were found in the KO mice. 1.0 ± 1.0% of the WT rod terminals were light (LT), whereas the KO mice had 10.7 ± 2.8% (n = 4 different mice per genotype; 75–100 terminals were evaluated per animal). Mice were 12 months of age. Data are expressed as mean ± SD.

Acknowledgments

We thank members of the Dean Bok laboratory (University of California-Los Angeles, Los Angeles, CA, USA) for their help in the perfusion experiments and Shelby Wilkinson for technical assistance. We thank Dianna Johnson (University of Tennessee Health Science Center, Memphis, TN, USA) for valuable discussions related to retinal synapses.

Supported by National Institutes of Health Grants EY00871, EY04149, P30EY021725, and P20RR017703 (REA) and EY10542 (WBT); Foundation Fighting Blindness (REA); Reynolds Oklahoma Aging Center (REA); Research to Prevent Blindness (Dean McGee Eye Institute and University of Nebraska Medical Center); Fight for Sight (MJVH); and Senior Scientific Investigator Award from Research to Prevent Blindness (WBT).

Disclosure: **L.D. Bennett**, None; **B.R. Hopiavuori**, None; **R.S. Brush**, None; **M. Chan**, None; **M.J. Van Hook**, None; **W.B. Thoreson**, None; **R.E. Anderson**, None

References

1. Edwards AO, Donoso LA, Ritter R III. A novel gene for autosomal dominant Stargardt-like macular dystrophy with homology to the SUR4 protein family. *Invest Ophthalmol Vis Sci*. 2001;42:2652–2663.
2. Zhang K, Kniazeva M, Han M, et al. A 5-bp deletion in ELOVL4 is associated with two related forms of autosomal dominant macular dystrophy. *Nat Genet*. 2001;27:89–93.
3. Donoso LA, Frost AT, Stone EM, et al. Autosomal dominant Stargardt-like macular dystrophy: founder effect and reassessment of genetic heterogeneity. *Arch Ophthalmol*. 2001;119:564–570.
4. Griesinger IB, Sieving PA, Ayyagari R. Autosomal dominant macular atrophy at 6q14 excludes CORD7 and MCDR1/PBCRA loci. *Invest Ophthalmol Vis Sci*. 2000;41:248–255.
5. Kniazeva M, Chiang MF, Morgan B, et al. A new locus for autosomal dominant stargardt-like disease maps to chromosome 4. *Am J Hum Genet*. 1999;64:1394–1399.
6. Agbaga M-P, Brush RS, Mandal MNA, Henry K, Elliott MH, Anderson RE. Role of Stargardt-3 macular dystrophy protein (ELOVL4) in the biosynthesis of very long chain fatty acids. *Proc Natl Acad Sci U S A*. 2008;105:12843–12848.
7. Harkewicz R, Du H, Tong Z, et al. Essential role of ELOVL4 protein in very long chain fatty acid synthesis and retinal function. *J Biol Chem*. 2012;287:11469–11480.
8. Barabas P, Liu A, Xing W, et al. Role of ELOVL4 and very long-chain polyunsaturated fatty acids in mouse models of Stargardt type 3 retinal degeneration. *Proc Natl Acad Sci U S A*. 2013;110:5181–5186.

9. Logan S, Agbaga MP, Chan MD, et al. Deciphering mutant ELOVL4 activity in autosomal-dominant Stargardt macular dystrophy. *Proc Natl Acad Sci U S A*. 2013;110:5446–5451.
10. Mandal MNAR, Wong PW, Gage PJ, Sieving PA, Ayyagari R. Characterization of mouse orthologue of ELOVL4: genomic organization and spatial and temporal expression. *Genomics*. 2004;83:626–635.
11. Vasireddy V, Uchida Y, Salem N Jr, et al. Loss of functional ELOVL4 depletes very long-chain fatty acids (> or =C28) and the unique omega-O-acylceramides in skin leading to neonatal death. *Hum Mol Genet*. 2007;16:471–482.
12. Li W, Sandhoff R, Kono M, et al. Depletion of ceramides with very long chain fatty acids causes defective skin permeability barrier function, and neonatal lethality in ELOVL4 deficient mice. *Int J Biol Sci*. 2007;3:120–128.
13. Furland NE, Oresti GM, Antollini SS, Venturino A, Maldonado EN, Aveldano MI. Very long-chain polyunsaturated fatty acids are the major acyl groups of sphingomyelins and ceramides in the head of mammalian spermatozoa. *J Biol Chem*. 2007;282:18151–18161.
14. Aveldaño MI, Sprecher H. Very long chain (C24 to C36) polyenoic fatty acids of the n-3 and n-6 series in dipolyunsaturated phosphatidylcholines from bovine retina. *J Biol Chem*. 1987;262:1180–1186.
15. Aveldaño MI. A novel group of very long chain polyenoic fatty acids in dipolyunsaturated phosphatidylcholines from vertebrate retina. *J Biol Chem*. 1987;262:1172–1179.
16. Bennett LD, Brush RS, Chan M, et al. Effect of reduced retinal VLC-PUFA on rod and cone photoreceptors. *Invest Ophthalmol Vis Sci*. 2014;55:3150–3157.
17. Buckley K, Kelly RB. Identification of a transmembrane glycoprotein specific for secretory vesicles of neural and endocrine cells. *J Cell Biol*. 1985;100:1284–1294.
18. Ueki Y, Wang J, Chollangi S, Ash JD. STAT3 activation in photoreceptors by leukemia inhibitory factor is associated with protection from light damage. *J Neurochem*. 2008;105:784–796.
19. Redburn DA, Thomas TN. Isolation of synaptosomal fractions from rabbit retina. *J Neurosci Methods*. 1979;1:235–242.
20. Martin RE, Elliott MH, Brush RS, Anderson RE. Detailed characterization of the lipid composition of detergent-resistant membranes from photoreceptor rod outer segment membranes. *Invest Ophthalmol Vis Sci*. 2005;46:1147–1154.
21. Busik JV, Reid GE, Lydic TA. Global analysis of retina lipids by complementary precursor ion and neutral loss mode tandem mass spectrometry. *Methods Mol Biol*. 2009;579:33–70.
22. Li F, Marchette LD, Brush RS, et al. DHA does not protect ELOVL4 transgenic mice from retinal degeneration. *Mol Vis*. 2009;15:1185–1193.
23. Asi H, Perlman I. Relationships between the electroretinogram a-wave, b-wave and oscillatory potentials and their application to clinical diagnosis. *Doc Ophthalmol*. 1992;79:125–139.
24. Ghosh KK, Bujan S, Haverkamp S, Feigenspan A, Wassle H. Types of bipolar cells in the mouse retina. *J Comp Neurol*. 2004;469:70–82.
25. Nawy S. Desensitization of the mGluR6 transduction current in tiger salamander On bipolar cells. *J Physiol*. 2004;558:137–146.
26. Wachtmeister L. Oscillatory potentials in the retina: what do they reveal. *Prog Retin Eye Res*. 1998;17:485–521.
27. Holcombe DJ, Lengefeld N, Gole GA, Barnett NL. The effects of acute intraocular pressure elevation on rat retinal glutamate transport. *Acta Ophthalmol*. 2008;86:408–414.
28. Sieving PA, Frishman LJ, Steinberg RH. Scotopic threshold response of proximal retina in cat. *J Neurophysiol*. 1986;56:1049–1061.
29. Frishman LJ, Steinberg RH. Light-evoked increases in [K+]o in proximal portion of the dark-adapted cat retina. *J Neurophysiol*. 1989;61:1233–1243.
30. Lombardini JB. Spontaneous and evoked release of [3H]taurine from a P2 subcellular fraction of the rat retina. *Neurochem Res*. 1993;18:193–202.
31. VanGuilder HD, Brucklacher RM, Patel K, Ellis RW, Freeman WM, Barber AJ. Diabetes downregulates presynaptic proteins and reduces basal synapsin I phosphorylation in rat retina. *Eur J Neurosci*. 2008;28:1–11.
32. Sherry DM, Wang MM, Bates J, Frishman LJ. Expression of vesicular glutamate transporter 1 in the mouse retina reveals temporal ordering in development of rod vs. cone and ON vs. OFF circuits. *J Comp Neurol*. 2003;465:480–498.
33. Cotman C, Blank ML, Moehl A, Snyder F. Lipid composition of synaptic plasma membranes isolated from rat brain by zonal centrifugation. *Biochemistry*. 1969;8:4606–4612.
34. Takamori S, Holt M, Stenius K, et al. Molecular anatomy of a trafficking organelle. *Cell*. 2006;127:831–846.
35. Lagali PS, Liu J, Ambasudhan R, et al. Evolutionarily conserved ELOVL4 gene expression in the vertebrate retina. *Invest Ophthalmol Vis Sci*. 2003;44:2841–2850.
36. Spiwoks-Becker I, Vollrath L, Seeliger MW, Jaissle G, Eshkind LG, Leube RE. Synaptic vesicle alterations in rod photoreceptors of synaptophysin-deficient mice. *Neuroscience*. 2001;107:127–142.
37. McCall MA, Gregg RG. Comparisons of structural and functional abnormalities in mouse b-wave mutants. *J Physiol*. 2008;586:4385–4392.
38. Sonntag S, Dedek K, Dorgau B, et al. Ablation of retinal horizontal cells from adult mice leads to rod degeneration and remodeling in the outer retina. *J Neurosci*. 2012;32:10713–10724.
39. Marc RE, Jones BW, Watt CB, Strettoi E. Neural remodeling in retinal degeneration. *Prog Retin Eye Res*. 2003;22:607–655.
40. Zhang XM, Yang Z, Karan G, et al. Elovl4 mRNA distribution in the developing mouse retina and phylogenetic conservation of Elovl4 genes. *Mol Vis*. 2003;9:301–307.
41. Grayson C, Molday RS. Dominant negative mechanism underlies autosomal dominant Stargardt-like macular dystrophy linked to mutations in ELOVL4. *J Biol Chem*. 2005;280:32521–32530.
42. Goetze B, Schmidt K-F, Lehmann K, Altrock WD, Gundelfinger ED, Löwel S. Vision and visual cortical maps in mice with a photoreceptor synaptopathy: reduced but robust visual capabilities in the absence of synaptic ribbons. *NeuroImage*. 2010;49:1622–1631.

Investigative Ophthalmology & Visual Science